



**ARTICLE**

## Synthesis and Properties of Rosin-Based Composite Acrylamide Hydrogels

Shuangsheng Zhang, Bin Sun, Siyu Li, Xiangyu Lin, Muhua Chen\* and Xu Xu\*

Jiangsu Co-Innovation Center of Efficient Processing and Utilization of Forest Resources, Jiangsu Provincial Key Laboratory for the Chemistry and Utilization of Agro-Forest Biomass, College of Chemical Engineering, Nanjing Forestry University, Nanjing, 210037, China

\*Corresponding Authors: Xu Xu. Email: xuxu200121@hotmail.com; Muhua Chen. Email: simonzrh@163.com

Received: 31 March 2022 Accepted: 06 May 2022

### ABSTRACT

Hydrogels have been widely applied in agricultural drought-resistance, pollution regulation, drug delivery and so on. Acrylamide (AM) is usually used as raw material to synthesize acrylamide hydrogels. However, inherently low mechanical strength greatly limits their applications in some special areas. Therefore, it is necessary to choose suitable functional monomers to optimize acrylamide hydrogels and improve their mechanical performances. In this paper, a novel acrylamide monomer modified by rosin was synthesized, and then polyacrylamide/rosin-based acrylamide (RAM) composite hydrogels were prepared via free radical polymerization using potassium persulfate as initiator, N, N'-methylene-bisacrylamide (MBA) as a crosslinker. The influence of RAM monomer was investigated in detail. The chemical structure, pore structure, swelling properties, thermal performances and mechanical properties of composite hydrogels were characterized by Fourier Transform Infrared spectrometer (FT-IR), thermogravimetric analysis (TG), scanning electron microscope (SEM), and universal testing, respectively. The results showed that the thermal stability and mechanical property of RAM hydrogels were improved significantly. The compressive strength of RAM hydrogels was increased to 3.5 times than that of AM hydrogels, and the tensile strength was 5.1 times compared with AM hydrogels as well. Moreover, RAM hydrogels exhibited a faster initial swelling rate due to the new pore structure formed after introducing the RAM monomer.

### KEYWORDS

Hydrogel; rosin; swelling property; mechanical property; thermal stability

## 1 Introduction

As an important organic material, acrylamide (AM) can be easily polymerized and copolymerized with other functional monomers. In industrial production, acrylamide has a wide scope of industrial applications, especially can participate in the polymerization reaction as a precursor to synthesize polyacrylamide (PAM) [1]. As we know, PAM has been widely applied in oil production technology, wastewater treatment processes, pulp and paper processing, mining, and mineral processing [2–6]. Besides, it can be used as raw material to prepare polyacrylamide hydrogels (PAMH) with high swelling, porosity, and high metal ion binding abilities [7–9]. In general, due to its three-dimensional crosslinked polymeric networks, PAMH can present pleasuring swell properties by absorbing substantial amounts of water from aqueous environments [10]. In recent years, PAMH has attracted great interest due to the features of strong hydrophilic and colorless, etc., which has been widely used as filler material, medicine ointment, drug



carrier and so on [11–14]. For example, Yang et al. [15] successfully prepared double-network (DN) hydrogels utilizing PAM hydrogels through a novel method, which open an avenue to fabricate multifarious and multifunctional DN hydrogels. Zhen et al. [16] took acrylamide as the precursor to compose PAAM/PA/PDA hydrogel via free-radical polymerization, and then conducted a porous polymer hydrogel-based electrochemical sensor for rapid detection of  $\text{Cu}^{2+}$ . It was found that the copolymer PAAM/PA/PDA hydrogel not only provided a large surface area for increasing the number of immobilized molecules/ions, but also exhibited a good conductivity. Zhang et al. [17] made use of polyacrylamide and calcium alginate (CA) to compose a hydrogel filtration membrane. The free-standing CA/PAM hydrogel filtration membrane exhibited excellent anti-fouling properties and had promising application prospects in the fields of protein separation, microorganism filtration and removal of dyes. Farahani et al. [18] developed an intelligent closed-loop insulin delivery system for implantation by polymerization of chitosan (CS), acrylamide (AAm) and polyethylene glycol (PEG).

Although polyacrylamide hydrogels possess a three-dimensional network of cross-linked structures and have tunable physicochemical properties [19], inherently low mechanical strength has greatly limited their applications [20]. As mentioned above, the low polymer density in swollen state is one of the reasons for the poor mechanical properties of the PAMH [21]. Thus, the application domain of acrylamide derivatives monomer was limited. It is imperative to develop a acrylamide monomer with unique structure for improving mechanical properties. The simplest approach to overcome the drawback is to introduce another functional monomer in PAMH. Therefore, different types of polymers have come up to supply the traditional acrylamide hydrogels.

In last decades, natural polymers have been primarily attractive because they are biodegradable, inexpensive, and readily available. Rosin is a mixture of a variety of resin acid isomers, which occurs naturally in oleoresins of pine trees, and its derivatives have been pharmaceutically evaluated as microencapsulating materials, film forming agents and as binding agents in formulation of tablets. The unique hydrogenated phenanthrene ring structure of rosin resin acid and the double bonds and carboxyl functional groups can provide a variety of reaction sites. As a result, rosin resin acids are easy to be chemically modified and they can take part in various reactions to synthesize functional monomers. Due to the stable large volume hydrogenated phenanthrene ring structure and its limiting effect on polymer molecular motion, the polymer materials modified by rosin resin acids usually own better mechanical properties and thermal stability. In this paper, a novel rosin-based monomer was synthesized, and then rosin-based acrylamide (RAM) composite hydrogels were prepared via free radical polymerization using potassium persulfate as initiator, N, N'-methylene-bisacrylamide (MBA) as a crosslinker. The chemical structure, swelling properties, thermal performances and mechanical properties of RAM composite hydrogels were investigated.

## 2 Experimental Section

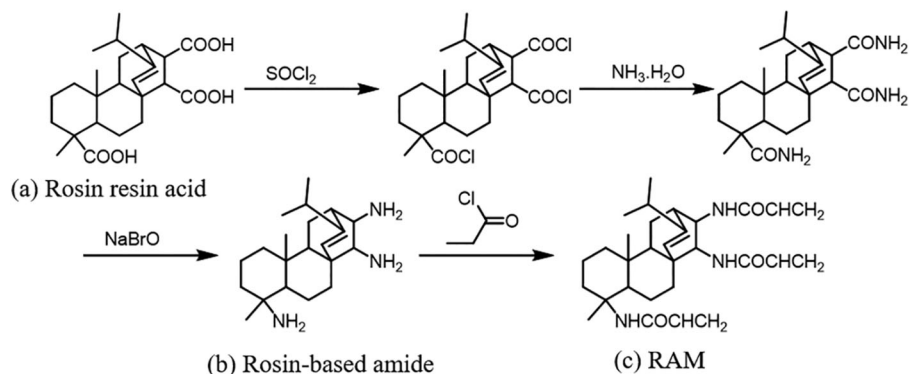
### 2.1 Material

The materials utilized in this work included acrylamide (AM), rosin resin acid (fumaroinmaric acid), potassium persulfate ( $\text{K}_2\text{S}_2\text{O}_8$ ), dichloromethane, acryloyl chloride, anhydrous sodium sulfate and so on. Acrylamide and potassium persulfate were purchased from Sinopharm Chemical Co. (China). The cross-linking agent N, N'-methylene bisacrylamide (MBA) was purchased from Sinopharm Chemical Co. (China). The dichloromethane, acryloyl chloride, and anhydrous sodium sulfate were also purchased from Shanghai Aladdin Biochemical Technology Co., Ltd. (China).

### 2.2 Synthesis of Rosin-Based Acrylamide Monomer (RAM)

As shown in [Scheme 1](#), firstly, the rosin-based amines (b) were synthesized utilizing rosin resin acid (a) according to a previously published article [22]. Then, 7 g (0.076 mol) of acryloyl chloride and 50 mL

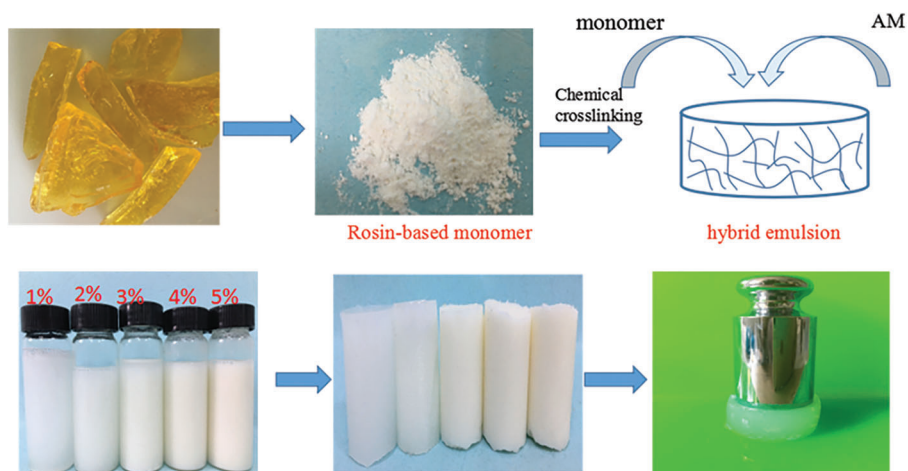
dichloromethane were added to a 250 mL three-port flask equipped with a condensing tube and thermometer in an ice salt bath. 8 g (0.024 mol) of rosin-based amines (b) was dissolved in 80 mL dichloromethane and dripped into the above three flasks using a constant pressure drop funnel. After dripping, the reaction was stirred for 30 min at room temperature. At the end of the reaction, the product was extracted with ethyl acetate/water system for three times, and the synthesized organic phase was dried by anhydrous sodium sulfate. The solvent was removed by vacuum distillation, and then the product was washed repeatedly and dried to obtain RAM monomer (c).



**Scheme 1:** Synthesis of RAM monomer

### 2.3 Synthesis of Composite Hydrogels

AM hydrogels were prepared via free radical polymerization. A reaction was conducted by adding MBA as a cross-linking agent (0.5 wt% with respect to hydrogels) and using potassium persulfate ( $K_2S_2O_8$ ) as an initiator. [Scheme 2](#) shows the synthesis of acrylamide hydrogels. Briefly, 20 g acrylamide was dissolved in 80 g deionized water containing 0.5% mass crosslinker (based on the number of hydrogels) and 0.05% mass initiator (based on the number of hydrogels). Finally, the reaction solution was poured into a glass flask and reacted at 60°C for 2 h. RAM composite hydrogels were prepared by mixing AM, MBA,  $K_2S_2O_8$ , and adding different ratio (1–5 wt%) of rosin-based monomer. Then, hydrogels were laced into the neutralized deionized water at 60°C. After the graft copolymerization reaction, RAM hydrogels were washed with plenty of water for several times, and then dried in an oven at 40°C. [Table 1](#) shows the distribution ratio of AM and RAM hydrogels.



**Scheme 2:** Synthesis of acrylamide hydrogels

**Table 1:** Distribution ratio of AM and RAM hydrogels

Samples	AM/wt%	RAM/wt%	H <sub>2</sub> O/wt%	MBA/wt%	KPS wt%
AM-5	5	/	95	0.5	0.5
AM-10	10	/	90	0.5	0.5
AM-15	15	/	85	0.5	0.5
AM-20	20	/	80	0.5	0.5
RAM-1	20	1	80	0.5	0.5
RAM-2	20	2	80	0.5	0.5
RAM-3	20	3	80	0.5	0.5
RAM-4	20	4	80	0.5	0.5
RAM-5	20	5	80	0.5	0.5

Notes: AM-a: a represents the mass fraction of AM monomer in AM aqueous solution in the AM hydrogels.  
RAM-b: b represents the mass fraction of RAM monomer in AM aqueous solution in the RAM hydrogels.

## 2.4 Characterization of Hydrogels

### 2.4.1 Thermal Property of Hydrogels

The thermal behavior of hydrogels was determined via thermo-gravimetric analyzer (TG). 5 mg dried samples were weighted and heated from room temperature to 800°C with 10 °C/min heating rate under nitrogen (flow of 100 mL/min) [23]. The weight losses against temperature were recorded as their matching thermograms and investigated the initial decomposition temperature of the sample.

### 2.4.2 Mechanical Performance of Hydrogel

Tensile and compression testing: The tensile and compression tests of different hydrogels were conducted by the universal testing machine with a constant speed of 5 mm·min<sup>-1</sup>. For tensile tests, the hydrogels were cut into a dumbbell shape using an ASTM-D638 type cutting die, and the tensile data was reported as stress *vs.* strain curve. For compression tests, the hydrogels were cut into the size with a height of 10 mm and a diameter of 24 mm, and the compression data was reported as compressive stress *vs.* compressive strain curve [24,25].

### 2.4.3 Swelling Properties

The swelling behaviors of RAM hydrogels were studied in detail. The swollen ( $W_s$ ) and dry ( $W_d$ ) weights were measured in an equilibrium state [26] ( $W_s$  was the weight of the swollen hydrogel for every 100 min and  $W_d$  was the weight of the dried hydrogel). Samples were removed from the buffer, blotted with filter paper, and swollen weight was recorded. The equilibrium swelling ratio (SR) was calculated as

$$SR = W_s / W_d$$

The swelling degree (SD) was valued at room temperature with the formula:  $SD = (W_s - W_d) / W_d$  [27].

### 2.4.4 Morphology of Hydrogels

Morphology of the AM hydrogels and rosin-based RAM hydrogels were observed by a scanning electron microscope (SEM; JSM 6390, JEOL, Japan). Before SEM observation, the hydrogels were freeze-dried to remove water thoroughly. The dried hydrogels were carefully sliced to expose the cross-sections and sputtered with gold before examination [28].

The pore structure analysis was conducted by Nitrogen adsorption instrument in the relative pressure  $P/P_0 = 0.95$ . Before the adsorption measurement, the hydrogels were freeze-dried for 1 day to remove

water thoroughly. The micropore volume was calculated according to DR equation. And the mesoporous volume was obtained by subtracting micropore volume from the total pore volume [29].

### 3 Results and Discussion

Firstly, in order to verify the successful synthesis of RAM monomer, the  $^1\text{H}$  NMR spectra of rosin and RAM monomer were conducted by nuclear magnetic resonance spectroscopy instrument (Bruker500 MHZ) to analyze the structure, as shown in Fig. 1. The peaks at 7.28, 7.00 and 6.85 ppm shown in the spectra are related to the proton of  $-\text{NH}-$  in RAM monomer. Besides, the characteristic peak around 11.00 ppm associated with  $-\text{COOH}$  of rosin disappears in RAM monomer, confirming the successful synthesis of RAM monomer.

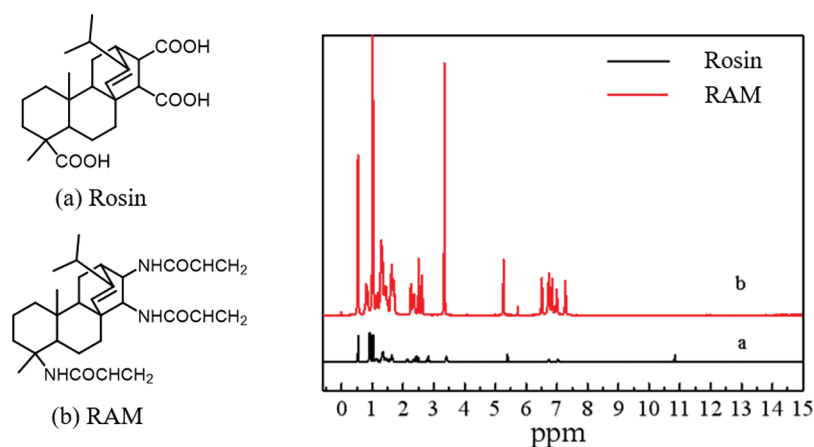


**Figure 1:**  $^1\text{H}$  NMR spectra of rosin resin acid (a) and RAM monomer (b)

Fig. 2 shows the FTIR spectra of hydrogels with wave number between  $4000$  and  $500\text{ cm}^{-1}$ . The observed N-H stretching bands at  $3100\text{ cm}^{-1}$  do exist in all the samples. As can be seen in the FTIR spectra of RAM hydrogels, the N-H stretching band can be observed at  $3340$  and  $3186\text{ cm}^{-1}$ , while the C-H absorption bands, C=O and C-N stretching bands belonging to acrylamide are observed at  $2928$ ,  $1647$ ,  $1410\text{ cm}^{-1}$ , respectively. The N-H bend vibration band of secondary amid and C=O stretching vibration band for RAM hydrogels can be observed at  $1500\sim 1640\text{ cm}^{-1}$  and  $1647\text{ cm}^{-1}$ , respectively.

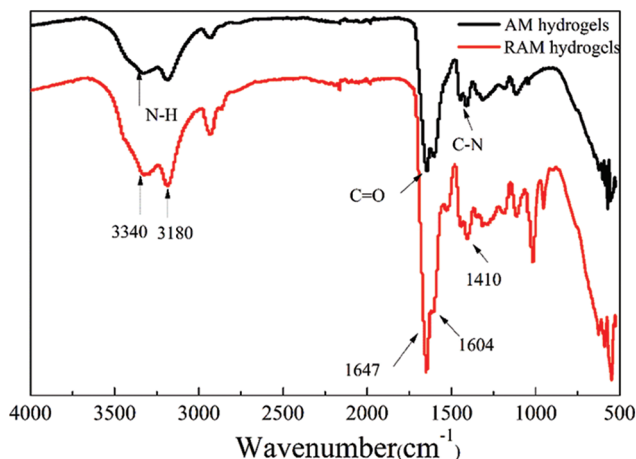


**Figure 2:** FTIR spectra of hydrogels

### 3.1 Thermal Performances of Hydrogels

The different TGA curves of AM hydrogels and RAM hydrogels are depicted in Fig. 3. The 5%, 50%, and maximum weight loss temperatures can be summarized from the picture. In the picture, the initial decomposition temper of the pure hydrogels sample (AM-20) is 130°C. After modification, the initial decomposition temper increases. For pure acrylamide hydrogels (AM-20), the first stage decomposition can be observed in the temperature range of 100°C–250°C with 20% weight loss. The maximum percentage weight loss can be observed in the temperature range of 250°C–400°C. Therefore, it can be stated that this stage of thermal decomposition is associated with the start of the breaking down of polymeric chain. In contrast, the TGA curves of RAM hydrogels involved the following steps: the desorption of adsorbed water, dehydration reactions and finally the depolymerization reactions because of the breakage of crosslinks between different polymeric chains. The final stage of decomposition in poly hydrogels from the poly-nuclear rosin-based structures can be attributed to the rapture of C=O and C-C bonds in the rings. As can be seen from the picture, the thermal stability of RAM hydrogels exhibits obvious improvement. For AM hydrogels sample (AM-20), the 5% weight loss temperatures were 128°C. The 50% weight loss temperatures is 380°C. After modification, the 50% weight loss temperatures improved. The highest temperature of 50% weight loss of hybrid hydrogel sample is 400°C. For RAM-4, the first stage decomposition is observed in the temperature range of 100°C–250°C and the weight loss is less than 10%. This stage of thermal decomposition is due to dehydration. The second stage decomposition is observed in the temperature range of 250°C–350°C with 30% weight loss occurring. This stage of thermal decomposition is associated with the breaking down of the crosslinks and different covalent bonds between different polymeric chains. The final stage decomposition is observed in the temperature range of 350°C–450°C with 70% weight loss. The final stage of decomposition may owe to the poly-nuclear rosin-based structures of composition. As for the DTG curve of hydrogel samples, the mass change ratio reaches to highest at 450°C for pure acrylamide hydrogel. After modification with the rosin-based monomer, the temperature of highest mass change is improved compared with pure acrylamide hydrogel (AM-20). The temperature of the biggest mass change of the hybrid hydrogel sample (RAM-5) was 465°C. The results above indicate that the stable large volume hydrogenated phenanthrene ring structure of rosin-based monomer limits the polymer molecular motion, resulting in better thermal properties of RAM hydrogels.

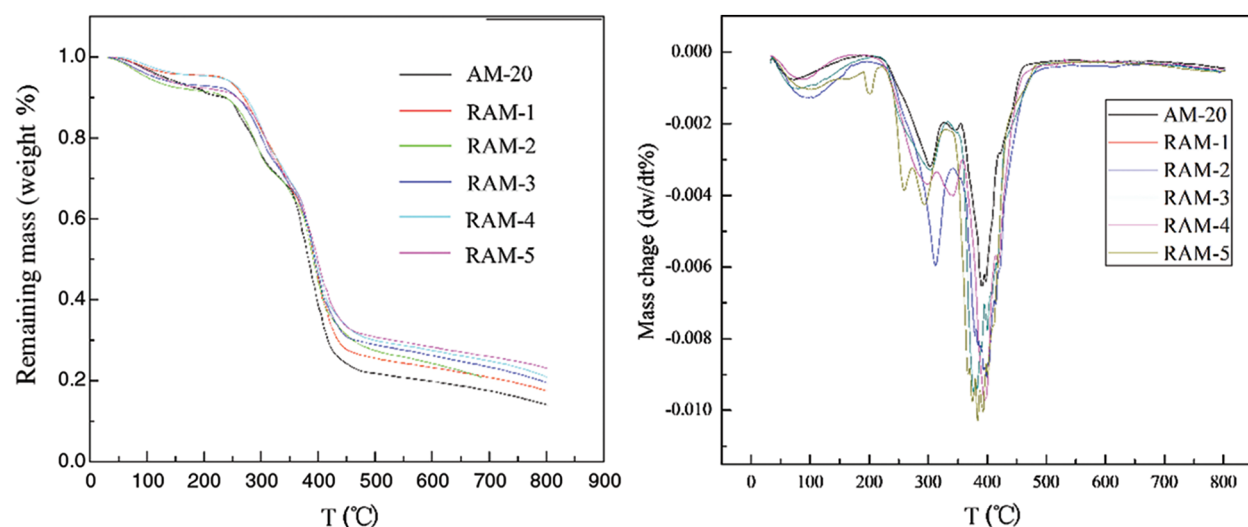
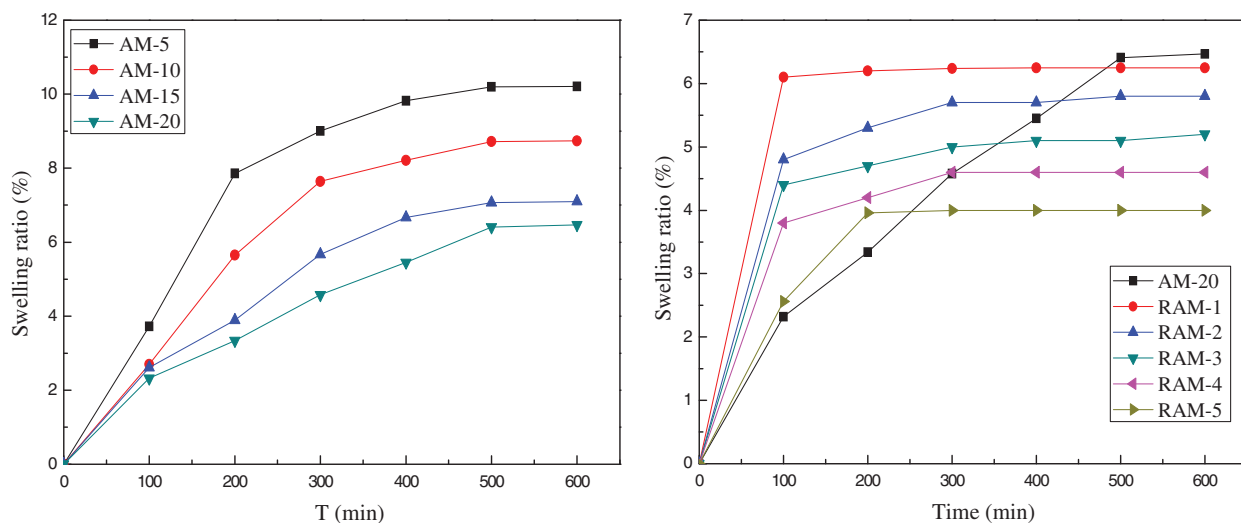


Figure 3: The TGA and DTG of Hydrogel samples

### 3.2 Swelling Behaviors of Hydrogels

Fig. 4 shows the swelling kinetics of hydrogels sample in deionized water. All hydrogels' samples are rapidly swelling in the first 100 min. As time goes on, the swelling ratios of AM hydrogels increase, and the swelling rates begin to be stable and reach the swelling equilibriums at 500 min. In addition, compared with AM hydrogels, the swelling kinetics curves of RAM hydrogels samples with the rosin-based monomer content of 1%, 2%, 3%, 4% and 5% own the faster swelling speed in the first 200 min.



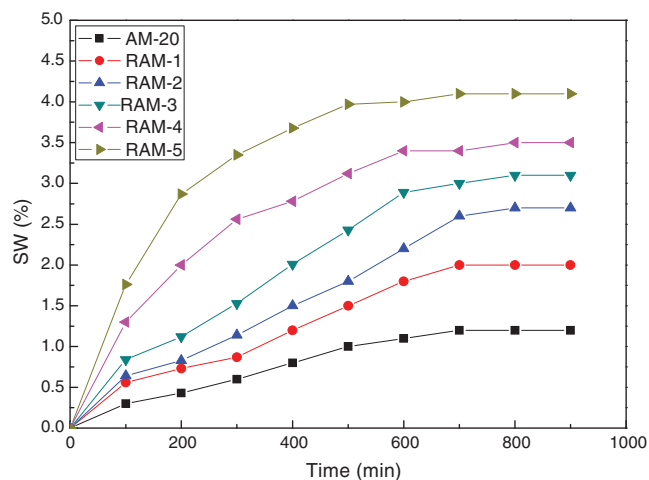
**Figure 4:** Swelling kinetics of hydrogel samples

Table 2 shows the swelling kinetics parameters of hydrogel samples. The initial swelling rate increases along with the addition of rosin-based monomer. When the rosin-based monomer content is 1%, the initial swelling rate is  $610 \times 10^{-3}$  g/min, which increased by 6 times compared with pure AM hydrogel. Otherwise, when the rosin-based monomer addition is 1%, the equilibrium swelling degree of composition hydrogel declines a little. Although the introduction of rosin-based copolymer reduces the water swelling ability, it can quickly reach a swelling balance. Therefore, RAM hydrogels can be applied in the field that needs to achieve swelling equilibrium quickly.

**Table 2:** Swell kinetics parameters of composite hydrogels

Samples	A	K ( $\times 10^{-3}$ g/min)	B	$Q_{eq}$ (g/g)
AM-5	2.688	372	0.0979	10.21
AM-10	3.704	270	0.114	8.74
AM-15	3.831	261	0.141	7.10
AM-20	4.310	232	0.155	6.47
RAM-1	1.639	610	0.160	6.25
RAM-2	2.083	480	0.172	5.8
RAM-3	2.273	440	0.192	5.2
RAM-4	2.632	380	0.217	4.6
RAM-5	3.906	256	0.250	4.0

Fig. 5 shows the swelling kinetics curves of hydrogel samples in the saturated salt solution. The RAM hydrogels in saturated salt water have a great increase in initial swelling rate and swelling capacity.



**Figure 5:** The swelling kinetics curve of hydrogel in saturated salt solution

### 3.3 Mechanical Properties of Hydrogels

Fig. 6 displays the mechanical behavior of the pure AM hydrogels and RAM hybrid hydrogels of uniaxial compression. For AM hydrogels, the compression mechanical properties become more excellent compared with the increase of acrylamide proportion. When the strain reaches 10% and 20%, the highest compress stress is 0.021 and 0.05 MPa. For RAM hydrogels, the mechanical properties are improved obviously. The largest compressive strength of RAM-2 can reach 0.058 MPa and 0.14 MPa with the strain of 10% and 20%, respectively, which is 2.8 times compared with pure AM hydrogels.

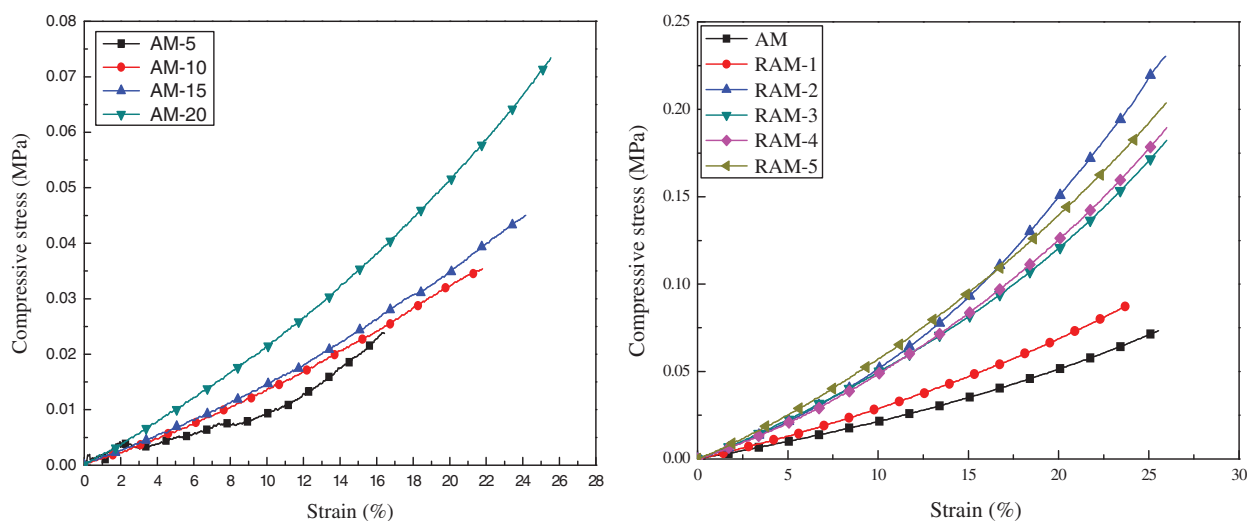


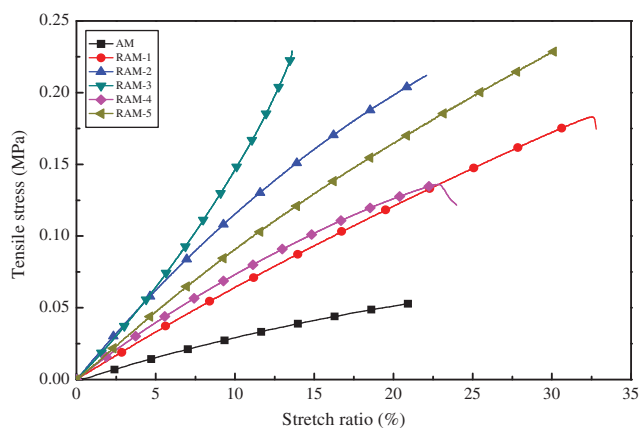
**Figure 6:** Engineering tensile stress vs. stretch ratio for AM hydrogels and RAM hydrogels

The mechanical properties of the hydrogels are summarized in Table 3. It can be observed that the compression strength increases greatly after introducing rosin-based monomer. When the strain is 10%, the parameter of elastic modulus ( $\epsilon_{10}$ ) increases gradually. And the maximum increase by a factor of 3.5.

**Table 3:** Mechanical properties of hydrogels

Samples	$\lambda$ at break (MPa)	$\sigma_e$ at break (MPa)	Elastic modulus ( $\epsilon_{10}$ ) MPa
AM-5	16	0.02	0.0010
AM-10	23	0.03	0.0014
AM-15	24	0.04	0.0016
AM-20	26	0.07	0.0020
RAM-1	24	0.087	0.0030
RAM-2	26	0.18	0.0054
RAM-3	26	0.19	0.0055
RAM-4	26	0.20	0.0056
RAM-5	26	0.22	0.0070

Pure AM hydrogels usually have poor mechanical properties. The tensile strength of AM hydrogel sample (AM-20) can be observed in the following Fig. 7, which shows the typical behavior expected for a loosely cross-linked network. For AM hydrogel sample (AM-20), when the stretch ratio is 10% and 15%, the tensile stress is 0.029 and 0.051 MPa. For RAM hydrogels, the tensile strength becomes optimized, and the tensile stress of RAM-5 is 0.12 and 0.20 MPa with the stretch ratio of 10% and 15%. Increased by a factor of 4.0.

**Figure 7:** Engineering tensile stress vs. stretch ratio for hydrogel samples

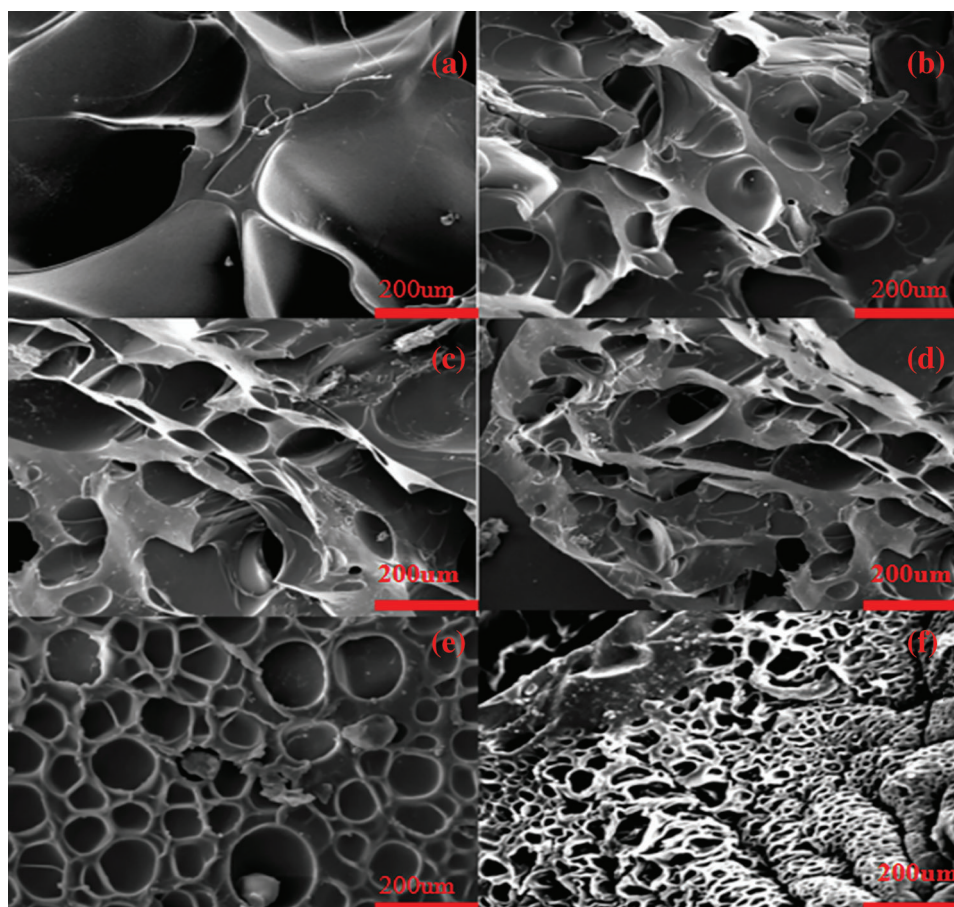
The mechanical properties of the hydrogels are summarized in Table 4. The parameters in Table 4 show that compression strength receive improvement after copolymerization with rosin-based monomer. When the strain is 10%, the parameter of elastic modulus ( $\epsilon_{10}$ ) increases gradually. The elastic modulus parameter of pure acrylamide hydrogel sample (AM-20) is 0.029 MPa, which increases to 0.15 MPa after modification, and becomes 5.1 times compared with pure AM hydrogels. The superior mechanical performances of RAM hydrogels can be attributed to the increase in the cross-linking density in the RAM composite hydrogels and the stable large volume hydrogenated phenanthrene ring structure of rosin-based monomer.

**Table 4:** Mechanical properties of hydrogels

Samples	$\lambda$ at break (MPa)	$\sigma_e$ at break (MPa)	Elastic modulus ( $\epsilon_{10}$ ) MPa
AM-5	16	0.02	0.0010
AM-10	23	0.03	0.0014
AM-15	24	0.04	0.0016
AM-20	26	0.07	0.0020
RAM-1	24	0.087	0.0030
RAM-2	26	0.18	0.0054
RAM-3	26	0.19	0.0055
RAM-4	26	0.20	0.0056
RAM-5	26	0.22	0.0070

### 3.4 Morphology of Hydrogels

The SEM images show the microstructures of the pure AM hydrogel and RAM hydrogels (Fig. 8) and a, b, c, d, e and f represent the SEM diagrams of AM-20, RAM-1, RAM-1, RAM-3, RAM-4 and RAM-5 hydrogels, respectively. The aperture of AM-20 is mainly concentrated around 500  $\mu\text{m}$ , which is a kind of loose microporous structure. For RAM hydrogels, with the increased content of rosin-based monomer, the prepared RAM composite hydrogels have more mesopores and small pores with the pore size concentrating on the range between 50 to 200  $\mu\text{m}$ , and the three-dimensional network structure of RAM hydrogel is more compact.

**Figure 8:** The SEM image of hydrogel samples

The BET analysis is applied to further characterize the pore structure of hydrogel samples. As shown in Fig. 9, the results reveal that mesopores are more developed as the concentration of acrylamide increased. Compared to pure AM hydrogels, RAM hydrogels exhibit higher microporous. Pure AM hydrogels present a size distribution from 5 to 10 nm, while the rosin-based RAM hydrogels have a size distribution from 2 to 5 nm, which also confirms the smaller pore structure and the more compact network of RAM hydrogels.

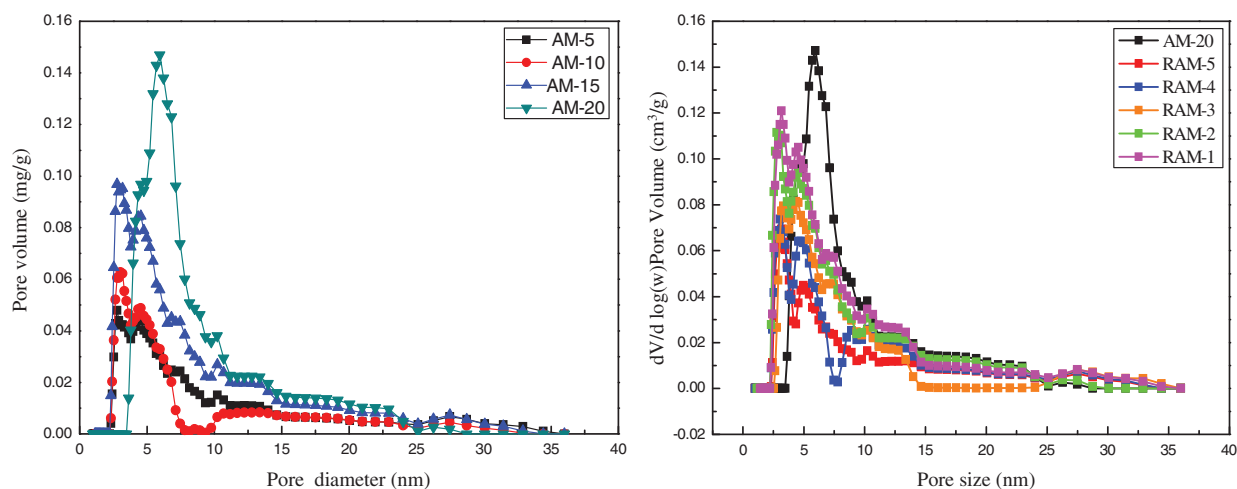


**Figure 9:** Pore size distribution of hydrogel samples

#### 4 Conclusion

In this paper, a novel acrylamide monomer modified by rosin was synthesized, and then polyacrylamide/rosin-based acrylamide (RAM) composite hydrogels were prepared via free radical polymerization using potassium persulfate as initiator, N, N'-methylene-bisacrylamide (MBA) as a crosslinker. The influence of adding RAM was investigated in detail. The RAM composite hydrogels exhibited better swelling properties, thermal performances, and mechanical properties. The initial swelling speed of RAM hydrogels became faster, which may be related to the new pore structure formed after copolymerization. The compressive strength of RAM hydrogels was increased to 3.5 times than that of AM hydrogels, and the tensile strength was 5.1 times compared with AM hydrogels as well. Moreover, RAM hydrogels exhibited the improved thermal stability after introducing the rosin-based components.

**Acknowledgement:** The authors gratefully acknowledge the project supported by National Natural Science Foundation of China, Top-Notch Academic Programs Project of Jiangsu Higher Education Institutions (ATPP) and the Priority Academic Program Development of Jiangsu Higher Education Institutions (PAPD).

**Funding Statement:** The project was supported by National Natural Science Foundation of China (32171722, 31470597 and 31600462).

**Conflicts of Interest:** The authors declare that they have no conflicts of interest to report regarding the present study.

#### References

1. Groll, J. (2016). Mechanically strong microstructured hydrogels based on reactive star-shaped prepolymers. *Macromolecular Symposia*, 358(1), 148–156. DOI 10.1002/masy.201500080.

2. Haq, M. A., Su, Y., Wang, D. (2017). Mechanical properties of PNIPAM based hydrogels: A review. *Materials Science & Engineering: C*, 70, 842–855. DOI 10.1016/j.msec.2016.09.081.
3. Shen, Y., Wang, H., Liu, Z., Li, W., Liu, Y. (2021). Fabrication of a water-retaining, slow-release fertilizer based on nanocomposite double-network hydrogels via ion-crosslinking and free radical polymerization. *Journal of Industrial and Engineering Chemistry*, 93, 375–382. DOI 10.1016/j.jiec.2020.10.014.
4. Cheng, L., Qin, Y., Su, Y., Pan, Y., Wang, Y. et al. (2022). Development of a high-strength and adhesive polyacrylamide gel for well plugging. *ACS Omega*, 7(7), 6151–6159. DOI 10.1021/acsomega.1c06626.
5. Wang, Y., Xiao, D., Quan, L., Chai, H., Sui, X. et al. (2022). Mussel-inspired adhesive gelatin-polyacrylamide hydrogel wound dressing loaded with tetracycline hydrochloride to enhance complete skin regeneration. *Soft Matter*, 18(3), 662–674. DOI 10.1039/D1SM01373D.
6. Deng, Y., Huang, M., Sun, D., Hou, Y., Li, Y. et al. (2018). Dual physically cross-linked  $\kappa$ -carrageenan-based double network hydrogels with superior self-healing performance for biomedical application. *ACS Applied Materials & Interfaces*, 10(43), 37544–37554. DOI 10.1021/acsami.8b15385.
7. Shi, F., Zhong, M., Zhong, L. (2017). Preparation of hierarchically crosslinked poly (acrylamide) hydrogels by assistance of crystallization of poly (vinyl alcohol). *Acta Polymerica Sinica*, 3, 491–497. DOI 10.11777/j.issn1000-3304.2017.16162.
8. Gan, S., Lin, W., Zou, Y., Xu, B., Zhang, X. (2020). Nano-hydroxyapatite enhanced double network hydrogels with excellent mechanical properties for potential application in cartilage repair. *Carbohydrate Polymers*, 229(8), 115523. DOI 10.1016/j.carbpol.2019.115523.
9. Yasmeen, N., Kalecki, J., Borowicz, P., Kutner, W. (2022). Electrochemically initiated synthesis of polyacrylamide microgels and core-shell particles. *ACS Applied Polymer Materials*, 4(1), 452–462. DOI 10.1021/acsapm.1c01359.
10. Seven, F., Sahiner, N. (2014). A simple post modification method for novel porous superabsorbent p(acrylamide) hydrogels and their H<sub>2</sub>. *production Journal of Polymer Research*, 21(12), 627. DOI 10.1007/s10965-014-0627-9.
11. Han, L., Xu, J., Lu, X. (2016). Biohybrid methacrylated gelatin/polyacrylamide hydrogels for cartilage repair. *Journal of Materials Chemistry B*, 5, 731–741. DOI 10.1039/c6tb02348g.
12. Metwally, M., Nguyen, T., Wiggins, H. (2022). Experimental lab approach for water based drilling fluid using polyacrylamide friction reducers to drill extended horizontal wells. *Journal of Petroleum Science and Engineering*, 212(2), 110132. DOI 10.1016/j.petrol.2022.110132.
13. Wu, S., Lou, D., Wang, H., Jiang, D., Fang, X. et al. (2022). One-pot synthesis of anti-freezing carrageenan/polyacrylamide double-network hydrogel electrolyte for low-temperature flexible supercapacitors. *Chemical Engineering Journal*, 435(2), 135057. DOI 10.1016/j.cej.2022.135057.
14. Zhu, M., Lu, D., Milani, A. H., Mahmoudi, N., King, S. M. et al. (2022). Comparing pH-responsive nanogel swelling in dispersion and inside a polyacrylamide gel using photoluminescence spectroscopy and small-angle neutron scattering. *Journal of Colloid and Interface Science*, 608(1), 378–385. DOI 10.1016/j.jcis.2021.09.163.
15. Yang, Y., Wang, X., Yang, F. (2016). A universal soaking strategy to convert composite hydrogels into extremely tough and rapidly recoverable double-network hydrogels. *Advanced Materials*, 28(33), 7178–7184. DOI 10.1002/adma.201601742.
16. Zhen, Z., Chen, H., Hua, Z. (2017). Polyacrylamide-phytic acid-polydopamine conducting porous hydrogel for rapid detection and removal of copper (II) ions. *Biosensors & Bioelectronics*, 91, 306. DOI 10.1016/j.bios.2016.12.047.
17. Zhang, X., Lin, B., Zhao, K. (2015). A free-standing calcium alginate/polyacrylamide hydrogel nanofiltration membrane with high anti-fouling performance: Preparation and characterization. *Desalination*, 365, 234–241. DOI 10.1016/j.desal.2015.03.015.
18. Farahani, B. V., Ghasemzadeh, H., Afraz, S. (2016). Intelligent semi-IPN chitosan-PEG-PAAm hydrogel for closed-loop insulin delivery and kinetic modeling. *Royal Society of Chemistry Advances*, 6(32), 26590–26598. DOI 10.1039/C5RA28188A.

19. Kumai, J., Sasagawa, S., Horie, M., Yui, Y. (2021). A novel method for polyacrylamide gel preparation using n-hydroxysuccinimide-acrylamide ester to study cell-extracellular matrix mechanical interactions. *Frontiers in Materials*, 8, 637278. DOI 10.3389/fmats.2021.637278.
20. Chen, N., Liu, W., Huang, J., Qiu, X. (2020). Preparation of octopus-like lignin-grafted cationic polyacrylamide flocculant and its application for water flocculation. *International Journal of Biological Macromolecules*, 146, 9–17. DOI 10.1016/j.ijbiomac.2019.12.245.
21. Versaevel, M., Grevesse, T., Riaz, M. (2014). Micropatterning hydroxy-PAAm hydrogels and Sylgard 184 silicone elastomers with tunable elastic moduli. *Methods in Cell Biology*, 121, 33. DOI 10.1016/B978-0-12-800281-0.00003-8.
22. Zhang, H., Huang, X., Jiang, J., Shang, S., Song, Z. (2017). Hydrogels with high mechanical strength cross-linked by a rosin-based crosslinking agent. *RSC Advances*, 7(67), 42541–42548. DOI 10.1039/C7RA08024G.
23. Kurumada, K., Suzuki, A., Baba, S. (2009). Relationship between polarity of template hydrogel and nanoporous structure replicated in sol-gel-derived silica matrix. *Journal of Applied Polymer Science*, 114(6), 4085–4090. DOI 10.1002/app.31095.
24. Zeng, R., Lu, S., Qi, C., Ji, L., Xu, J. et al. (2021). Polyacrylamide/carboxymethyl chitosan double-network hydrogels with high conductivity and mechanical toughness for flexible sensors. *Journal of Applied Polymer Science*, 139(16), e51993. DOI 10.1002/app.51993.
25. Zhang, B., Tang, H., Chen, J., Shen, Y., Shi, W. (2021). New mechanistic insights into the effect of cations on membrane fouling caused by anionic polyacrylamide. *Journal of Colloid and Interface Science*, 606(1–2), 10–21. DOI 10.1016/j.jcis.2021.07.148.
26. Yuan, N., Xu, L., Wang, H. (2016). Dual physically cross-linked double network hydrogels with high mechanical strength, fatigue resistance, notch-insensitivity, and self-healing properties. *ACS Applied Materials & Interfaces*, 1944, 34034–34044. DOI 10.1021/acsami.6b12243.
27. Zhang, Y., Zhao, X., Yang, W., Jiang, W., Fu, Q. (2020). Enhancement of mechanical property and absorption capability of hydrophobically associated polyacrylamide hydrogels by adding cellulose nanofiber. *Materials Research Express*, 7(1), 15319. DOI 10.1088/2053-1591/ab6373.
28. Yi, G., Huang, Y., Xiong, F. (2011). Preparation and swelling behaviors of rapid responsive semi-IPN NaCMC/PNIPAm hydrogels. *Journal of Wuhan University of Technology–Materials Science Edition*, 26(6), 1073–1078. DOI 10.1007/s11595-011-0365-3.
29. Huang, S., Li, Z., Chen, C., Tang, S., Cheng, X. et al. (2020). Synergetic activation of persulfate by heat and Fe (II)-complexes for hydrolyzed polyacrylamide degradation at high pH condition: Kinetics, mechanism, and application potential for filter cake removal during cementing in CO<sub>2</sub> storage wells. *Science of the Total Environment*, 713, 1–15. DOI 10.1016/j.scitotenv.2020.136561.